Preferential recognition of avian-like receptors in human influenza A H7N9 viruses

Rui Xu[1], Robert P. de Vries[2,3], Xueyong Zhu[1], Corwin M. Nycholat[2,3], Ryan McBride[2,3], Wenli Yu[1], James C. Paulson[2,3†], Ian A. Wilson[1,4†]

[1]Department of Integrative Structural and Computational Biology, The Scripps Research Institute, 10550 North Torrey Pines Road, La Jolla, CA 92037, USA.
[2]Department of Cell and Molecular Biology, The Scripps Research Institute, 10550 North Torrey Pines Road, La Jolla, CA 92037, USA.
[3]Department of Chemical Physiology, The Scripps Research Institute, 10550 North Torrey Pines Road, La Jolla, CA 92037, USA.
[4]Skaggs Institute for Chemical Biology, The Scripps Research Institute, 10550 North Torrey Pines Road, La Jolla, CA 92037, USA

† To whom correspondence should be addressed. E-mail: wilson@scripps.edu, jpaulson@scripps.edu

Supporting Online Material

Materials and Methods

Expression and purification of H7 HA in a baculovirus system

H7 HA cDNAs of H7N9 A/Shanghai/1/13 (Sh1) [Global Initiative on Sharing All Influenza Data (GISAID) isolate ID: EPI_ISL_138737] and H7N9 A/Shanghai/2/13 (Sh2) (GISAID isolate ID: EPI_ISL_138738) were synthesized by Genscript (USA) without codon optimization. H7 HA ectodomains were expressed using a baculovirus expression system as described previously (*21*). The constructs contain an N-terminal signal sequence for secretion, the H7 HA ectodomain, a thrombin cleavage site, a trimerization foldon sequence, and a His_6-tag for purification. Expressed HA was purified through a His-tag affinity purification step and subsequent column chromatography steps.

Crystallization and structural determination of H7 HA

The purified H7 HA was digested with thrombin to remove the expression tag, foldon and His tag. The product was purified by gel filtration in 20 mM Tris pH 8.0, 50 mM NaCl, and concentrated to 10 mg/mL for crystallization. H7 HA crystals were grown at 22.5°C in sitting drops by vapor diffusion against a reservoir containing 17-20% PEG3350, 0.2 M ammonium acetate. The crystals were cryoprotected by adding ethylene glycol to the mother liquor to a final concentration of 20%, and then flash cooling the crystals in liquid nitrogen. HA-ligand complexes were obtained by soaking HA crystals in cryo-solutions containing glycan ligands. Final ligand concentrations and soaking times are included in tables S1 and S2. Diffraction data were collected on synchrotron radiation sources specified in the data processing and refinement statistics in tables S1 and S2. Data were processed with HKL2000 (*40*). Initial phases were determined by molecular replacement using Phaser (*41*). Refinement was carried out in Phenix (*42*), and alternated with manual rebuilding and adjustment in COOT (*43*). Two HA protomers are present per asymmetric unit, one of which is much better defined in the electron density maps with lower B-values (fig. S4, tables S1-2). Final refinement statistics are summarized in tables

S1-2.

Expression and purification of H7 HA in a mammalian expression system

Codon-optimized H7 and H1 HA-encoding cDNAs (Genscript, USA) of A/Shanghai/2/13 (H7N9) and A/Kentucky/UR06-0258/2007 (H1N1) (GenBank accession number: CY028163) were cloned into the pCD5 expression plasmid as described previously (*44*). The pCD5 expression vector is adapted, such that the HA-encoding cDNAs are cloned in frame with DNA sequences coding for a signal sequence, a GCN4 trimerization motif (RMKQIEDKIEEIESKQKKIENEIARIKK) (*45*), and a Strep-tag II (WSHPQFEK; IBA, Germany).

The HA proteins were expressed in HEK293S GnTI$^-$ cells and purified from the cell culture supernatants as described previously (*46*). pCD5 expression vectors were transfected into HEK293S GnTI$^-$ cells using polyethyleneimine I (PEI). At 6 h post transfection, the transfection mixture was replaced by 293 SFM II expression medium (Gibco), supplemented with sodium bicarbonate (3.7 g/liter), glucose (2.0 g/liter), Primatone RL-UF (3.0 g/liter), penicillin (100 units/ml), Streptomycin (100 μg/ml), glutaMAX (Gibco), and 1.5% DMSO. Tissue culture supernatants were harvested 5–6 days post transfection. HA proteins were purified using Strep-Tactin Sepharose beads according to the manufacturer's instructions (IBA, Germany).

Plate-based glycan binding of HA from mammalian expression

96-well nunc maxisorp plates were coated with 1 μg/ml SLNLN that contained either α2-3 or α2-6 linked sialic acids. Purified, soluble trimeric HA was pre-complexed with horseradish peroxidase (HRP)-linked anti-Strep-tag mouse antibody and with HRP-linked anti-mouse IgG (4:2:1 molar ratio) prior to incubation for 15 minutes on ice. The pre-formed HA complexes were incubated for 90 minutes on the SLNLN-coated plates and washed three times with PBST, and HA binding was detected using the TMB substrate kit (Thermo Scientific), similar to our previously published protocols (*44*).

Glycan microarray binding of mammalian-expressed HA

HA samples were eluted from the strep tag beads with 100mM Tris, 150mM NaCl, 1mM EDTA, 2.5mM D-Biotin, pH 7.2. Purified soluble trimeric HA was used at 50μg/ml pre-complexed with horseradish peroxidase (HRP)-linked anti-Strep-tag mouse antibody and with Alexa488-linked anti-mouse IgG (4:2:1 molar ratio) prior to incubation for 15 min on ice in 100 μl PBS-T, and incubated on the array surface in a humidified chamber for 90 minutes. Slides were subsequently washed by successive rinses with PBS-T, PBS, and deionized H2O. Washed arrays were dried by centrifugation and immediately scanned for FITC signal on a Perkin-Elmer ProScanArray Express confocal microarray scanner. Fluorescent signal intensity was measured using Imagene (Biodiscovery) and mean intensity minus mean background was calculated and graphed using MS Excel. For each glycan, the mean signal intensity is calculated from 6 replicates. The highest and lowest signals of the 6 replicates were removed and the remaining 4 replicates were used to calculate the mean signal, standard deviation (SD), and standard error measurement (SEM). Bar graphs represent the averaged mean signal minus background for each glycan sample and error bars are the SD value. A list of glycans on the microarray is included in table S3.

Glycan microarray binding using baculovirus-expressed HAs

HA samples were dialyzed against 20 mM Tris-HCl, 50 mM NaCl, pH 8.0 overnight at 4^{o}C after His-tag affinity purification. Proteins were concentrated to 1 mg/ml before binding assay. Procedures for the HA glycan microarray binding assay were similar to those described above with small alterations. Briefly, 15 μg/ml HA was pre-complexed with an Alexa488-linked anti-penta-His mouse antibody and with Alexa488-linked anti-mouse IgG (4:2:1 molar ratio) and applied directly to the array for 1 hour.

Glycan binding of baculovirus-expressed HAs by bio-layer interferometry

Recombinant HA expression from the baculovirus expression system was buffer-exchanged into PBS buffer. Association of HA was measured on an Octet Red (ForteBio) against immobilized glycans on the sensors. 3′-SLNLN and 6′-SLNLN are biotinylated glycans and were immobilized using Super Streptavidin Biosensors (ForteBio). Association was measured for 300 seconds at 30°C by exposing the sensors to protein solution in 1x kinetic buffer (1x PBS, pH 7.4, 0.01% BSA, and 0.002% Tween 20) after which the sensors were exposed to 1x kinetic buffer for dissociation for 300 seconds at 30°C.

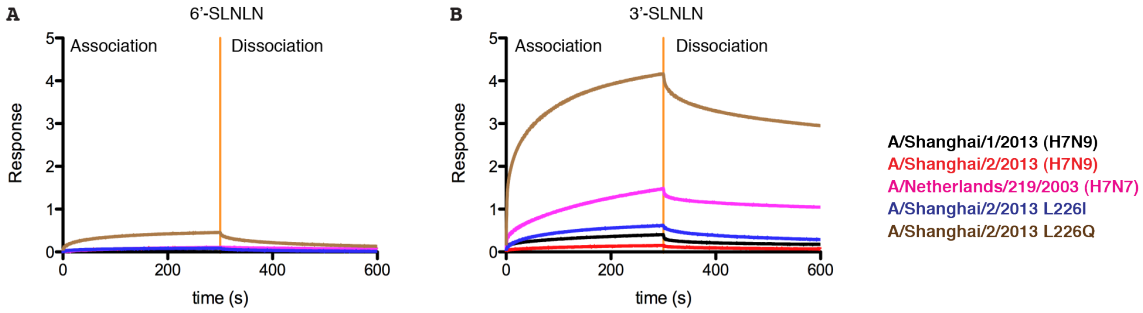

C

6'-SLNLN		
HA	KD1(μM)	KD2(μM)
A/Shanghai/1/2013 (H7N9)	N.D.	
A/Shanghai/2/2013 (H7N9)	N.D.	
A/Netherlands/219/2003(H7N7)	N.D.	
A/Shanghai/2/2013 L226I	N.D.	
A/Shanghai/1/2013 L226Q	>1	

3'-SLNLN		
HA	KD1(μM)	KD2(μM)
A/Shanghai/1/2013 (H7N9)	>1	
A/Shanghai/2/2013 (H7N9)	>1	
A/Netherlands/219/2003(H7N7)	0.24	0.88
A/Shanghai/2/2013 L226I	>1	
A/Shanghai/1/2013 L226Q	0.024	0.3

Fig. S1. Glycan binding specificity of the HAs was analyzed by Bio-Layer Interferometry (BLI) on an Octet Red system (ForteBio) using recombinant HAs expressed in a baculovirus system. HA binding at 0.7 mg/ml was measured against immobilized biotinylated glycans 6′-SLNLN (**A**), and 3′-SLNLN (**B**). (**C**) The binding curve for 3′-SLNLN was best fitted using the 2:1 heterogeneous ligand binding model, with apparent K_D values of 0.24 and 0.88 μM. Avian H7N7 HA (A/Netherlands/219/2003, Neth219) shows specific recognition for 3′-SLNLN, but not 6′-SLNLN. Sh1 and Sh2 HAs from the recent H7N9 human outbreak also display detectable binding but to 3′-SLNLN only, albeit less efficiently than Neth219 HA. The L226I mutation on the Sh2 background has little impact on receptor binding specificity or avidity. The L226Q mutant, however, shows much more efficient association with glycan 3′-SLNLN (apparent K_D values of 0.024 and 0.3μM).

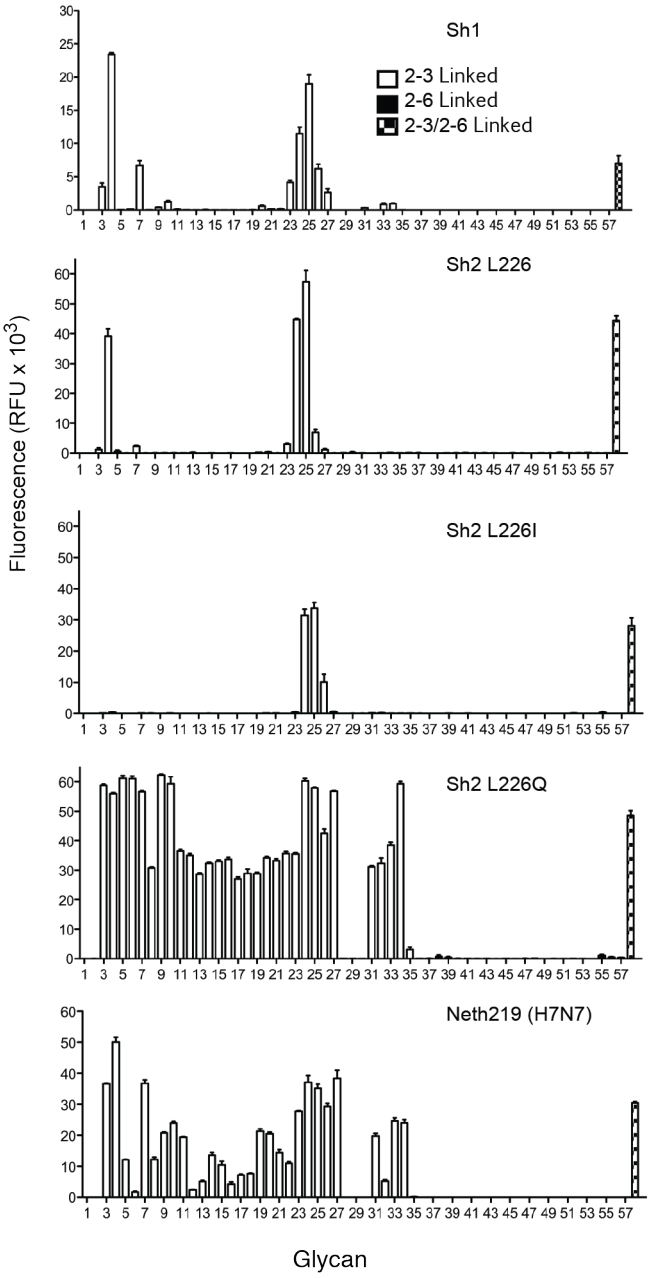

Fig. S2. Binding results on the glycan microarray using recombinant HA proteins from baculovirus expression. The mean signal and standard error were calculated from six independent replicates on the array. α2-3 sialosides are shown in white bars (glycans #3-35), α2-6 in black bars (glycans #36-56, very little signal), and stripped bars denoted mixed bi-antennary glycans (glycans #57-58) that contain both α2-3 and α2-6 linked sialylated glycans. List of glycans imprinted on the array is included in table S3.

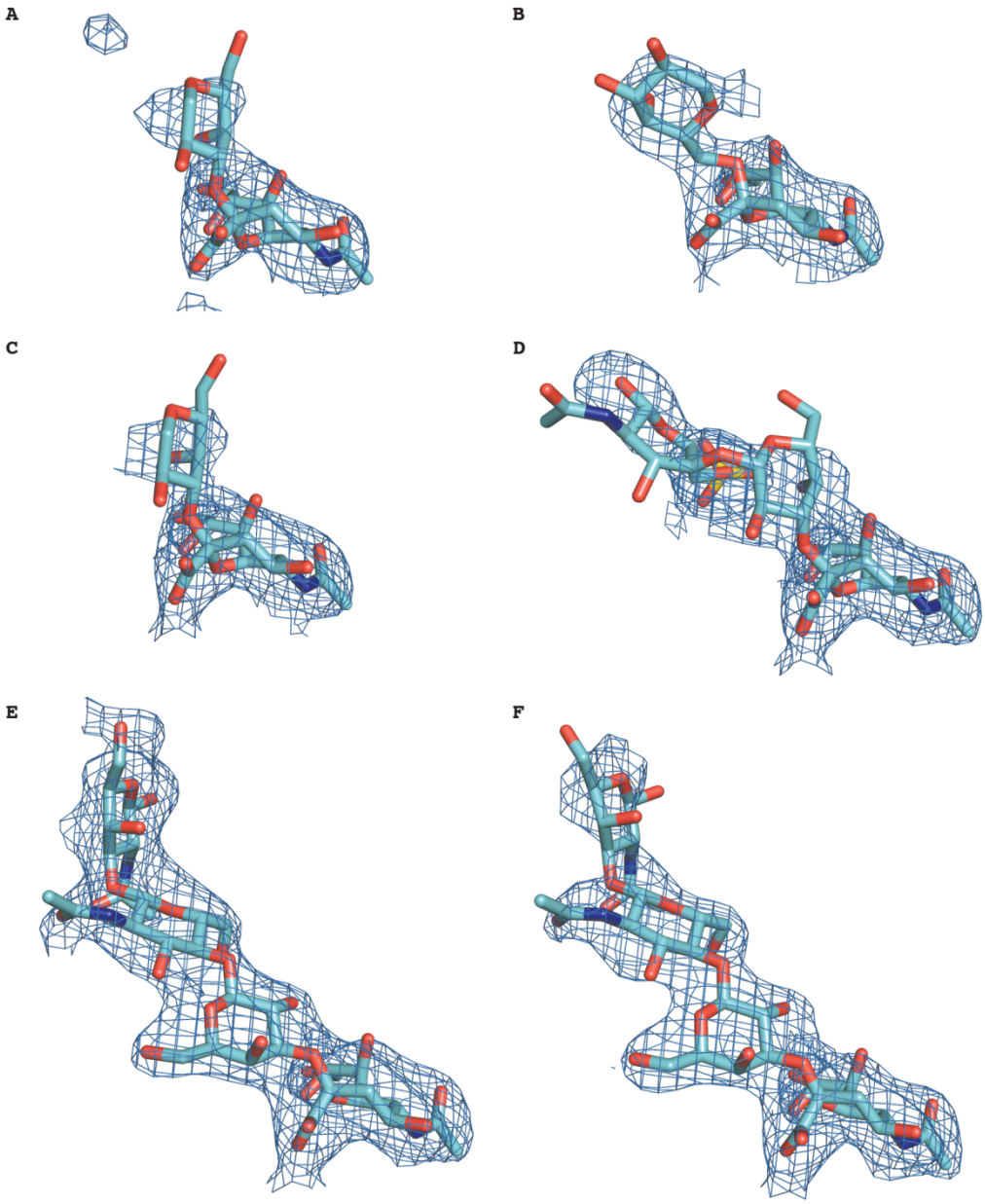

Fig. S3. Electron density maps (2Fo-Fc) of glycan ligands in the Sh2 H7 HA crystal structures. (**A**) LSTa, with 10 min soak (**B**) LSTc with 10 min soak (**C**) LSTa with 2 hour soak, (**D**) glycan #3, (**E**) glycan #21, (**F**) glycan #23. **D-F** are also 2 hour ligand soaks. The maps are contoured at a 1σ level (colored in grey) in panels **B**, **D E** and **F**. In (**A**) and (**C**), maps are shown at the 0.8σ level. Only density for the glycan receptors is shown for clarity.

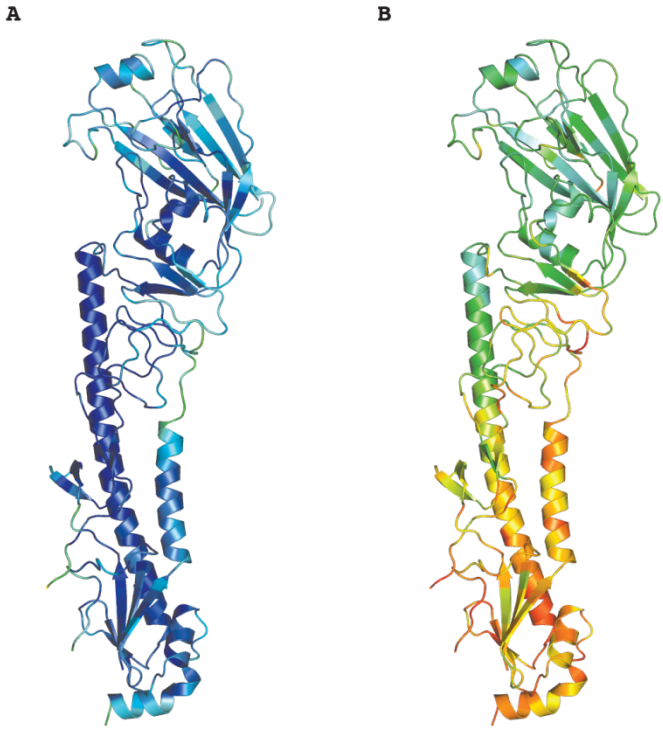

Fig. S4. Analysis of B-value distribution in the Sh2 H7 HA crystal structure. The two HA protomers within the asymmetric unit are colored by B-value. The warmest colors (*i.e.*, red and orange) indicate high B-values, while cool colors (*i.e.*, blue) indicate low B-values. The two protomers are shown in similar orientations for clarity. One protomer (**A**) has low B-values and clear and unambiguous electron density, while the other protomer (**B**) is less well-defined and has much higher B-values.

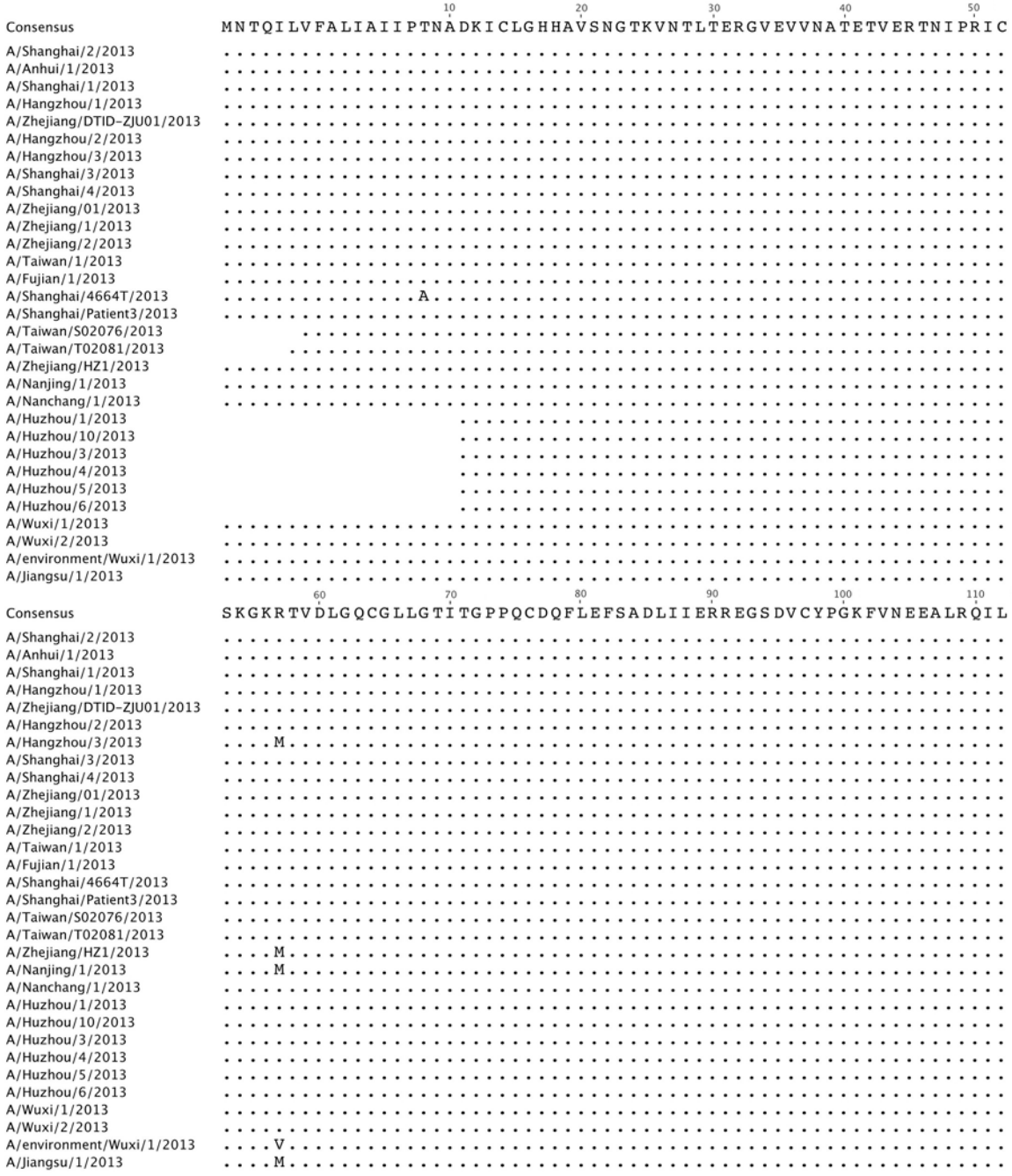
10 20 30 40 50
Consensus MNTQILVFALIAIIPTNADKICLGHHAVSNGTKVNTLTERGVEVVNATETVERTNIPRIC
A/Shanghai/2/2013
A/Anhui/1/2013
A/Shanghai/1/2013
A/Hangzhou/1/2013
A/Zhejiang/DTID-ZJU01/2013
A/Hangzhou/2/2013
A/Hangzhou/3/2013
A/Shanghai/3/2013
A/Shanghai/4/2013
A/Zhejiang/01/2013
A/Zhejiang/1/2013
A/Zhejiang/2/2013
A/Taiwan/1/2013
A/Fujian/1/2013
A/Shanghai/4664T/2013
A/Shanghai/Patient3/2013
A/Taiwan/S02076/2013
A/Taiwan/T02081/2013
A/Zhejiang/HZ1/2013
A/Nanjing/1/2013
A/Nanchang/1/2013
A/Huzhou/1/2013
A/Huzhou/10/2013
A/Huzhou/3/2013
A/Huzhou/4/2013
A/Huzhou/5/2013
A/Huzhou/6/2013
A/Wuxi/1/2013
A/Wuxi/2/2013
A/environment/Wuxi/1/2013
A/Jiangsu/1/2013
60 70 80 90 100 110
Consensus SKGKRTVDLGQCGLLGTITGPPQCDQFLEFSADLIIERREGSDVCYPGKFVNEEALRQIL
A/Shanghai/2/2013
A/Anhui/1/2013
A/Shanghai/1/2013
A/Hangzhou/1/2013
A/Zhejiang/DTID-ZJU01/2013
A/Hangzhou/2/2013
A/Hangzhou/3/2013
A/Shanghai/3/2013
A/Shanghai/4/2013
A/Zhejiang/01/2013
A/Zhejiang/1/2013
A/Zhejiang/2/2013
A/Taiwan/1/2013
A/Fujian/1/2013
A/Shanghai/4664T/2013
A/Shanghai/Patient3/2013
A/Taiwan/S02076/2013
A/Taiwan/T02081/2013
A/Zhejiang/HZ1/2013
A/Nanjing/1/2013
A/Nanchang/1/2013
A/Huzhou/1/2013
A/Huzhou/10/2013
A/Huzhou/3/2013
A/Huzhou/4/2013
A/Huzhou/5/2013
A/Huzhou/6/2013
A/Wuxi/1/2013
A/Wuxi/2/2013
A/environment/Wuxi/1/2013
A/Jiangsu/1/2013

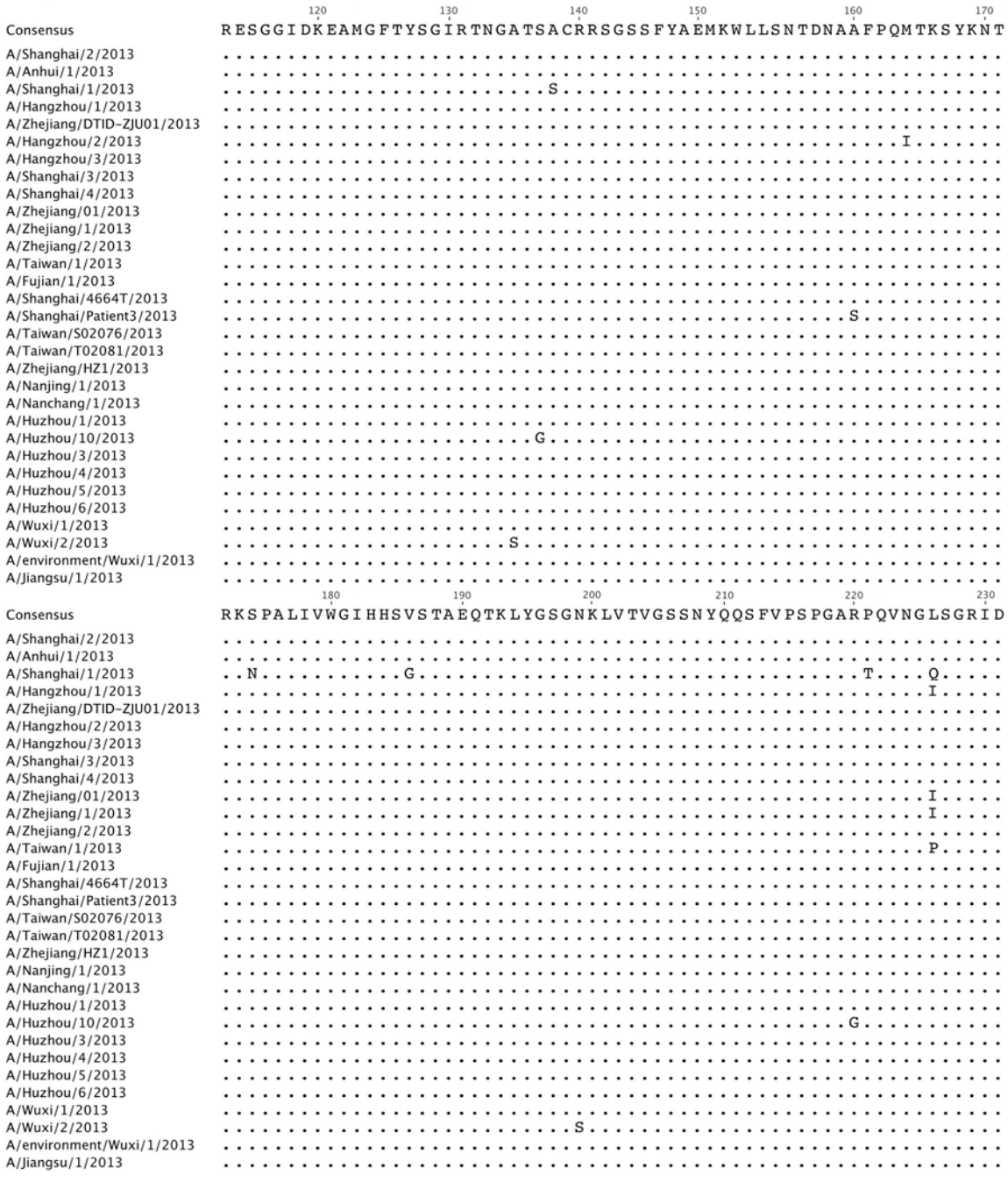
120 130 140 150 160 170
Consensus R E S G G I D K E A M G F T Y S G I R T N G A T S A C R R S G S S F Y A E M K W L L S N T D N A A F P Q M T K S Y K N T
A/Shanghai/2/2013
A/Anhui/1/2013
A/Shanghai/1/2013 S
A/Hangzhou/1/2013
A/Zhejiang/DTID-ZJU01/2013
A/Hangzhou/2/2013 I
A/Hangzhou/3/2013
A/Shanghai/3/2013
A/Shanghai/4/2013
A/Zhejiang/01/2013
A/Zhejiang/1/2013
A/Zhejiang/2/2013
A/Taiwan/1/2013
A/Fujian/1/2013
A/Shanghai/4664T/2013
A/Shanghai/Patient3/2013 S
A/Taiwan/S02076/2013
A/Taiwan/T02081/2013
A/Zhejiang/HZ1/2013
A/Nanjing/1/2013
A/Nanchang/1/2013
A/Huzhou/1/2013
A/Huzhou/10/2013 G
A/Huzhou/3/2013
A/Huzhou/4/2013
A/Huzhou/5/2013
A/Huzhou/6/2013
A/Wuxi/1/2013
A/Wuxi/2/2013 S
A/environment/Wuxi/1/2013
A/Jiangsu/1/2013
180 190 200 210 220 230
Consensus R K S P A L I V W G I H H S V S T A E Q T K L Y G S G N K L V T V G S S N Y Q Q S F V P S P G A R P Q V N G L S G R I D
A/Shanghai/2/2013
A/Anhui/1/2013
A/Shanghai/1/2013 N G T Q
A/Hangzhou/1/2013 I
A/Zhejiang/DTID-ZJU01/2013
A/Hangzhou/2/2013
A/Hangzhou/3/2013
A/Shanghai/3/2013
A/Shanghai/4/2013
A/Zhejiang/01/2013 I
A/Zhejiang/1/2013 I
A/Zhejiang/2/2013
A/Taiwan/1/2013 P
A/Fujian/1/2013
A/Shanghai/4664T/2013
A/Shanghai/Patient3/2013
A/Taiwan/S02076/2013
A/Taiwan/T02081/2013
A/Zhejiang/HZ1/2013
A/Nanjing/1/2013
A/Nanchang/1/2013
A/Huzhou/1/2013
A/Huzhou/10/2013 G
A/Huzhou/3/2013
A/Huzhou/4/2013
A/Huzhou/5/2013
A/Huzhou/6/2013
A/Wuxi/1/2013
A/Wuxi/2/2013 S
A/environment/Wuxi/1/2013
A/Jiangsu/1/2013

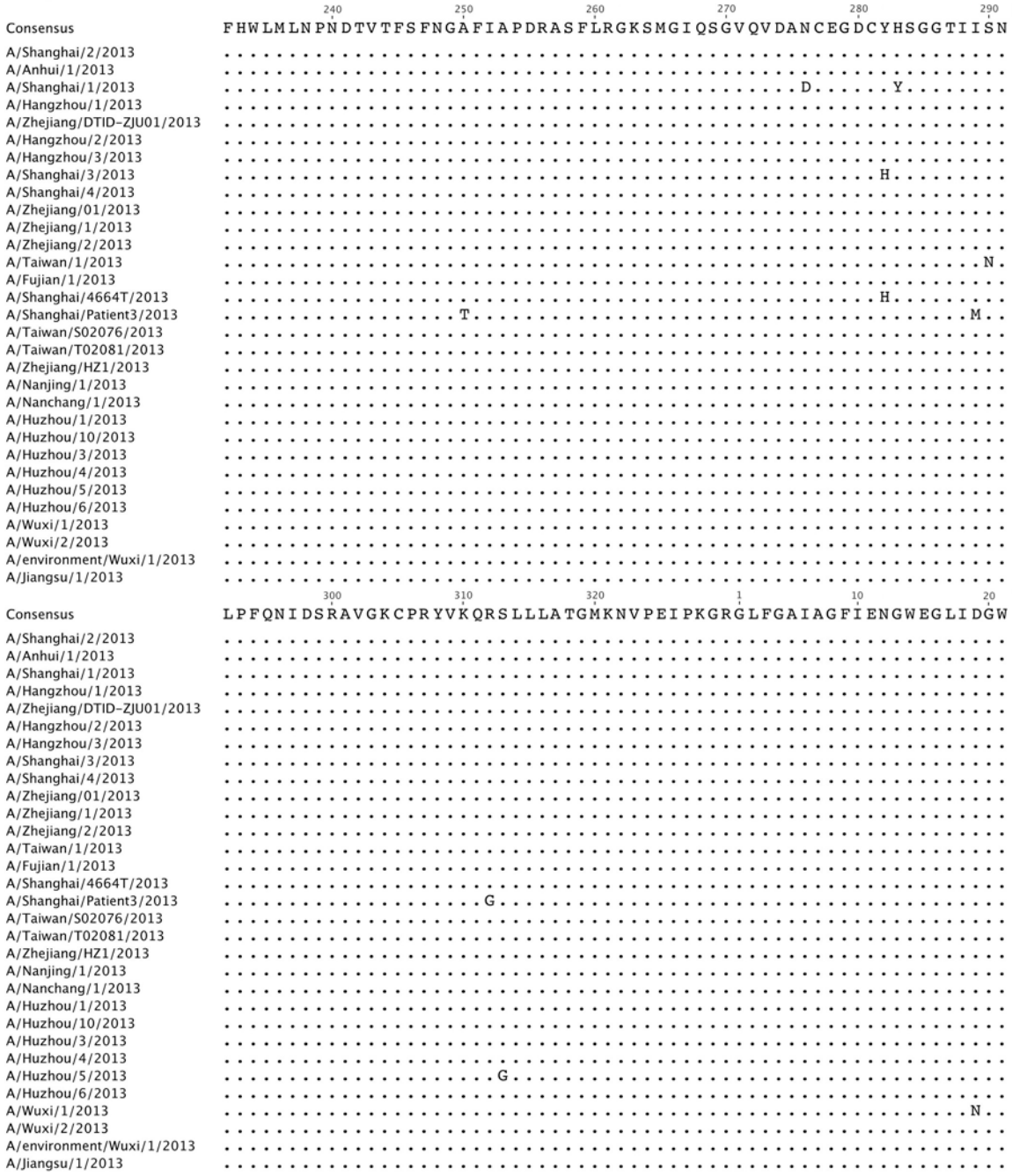
240 250 260 270 280 290
Consensus FHWLMLNPNDTVTFSFNGAFIAPDRASFLRGKSMGIQSGVQVDANCEGDCYHSGGTIISN
A/Shanghai/2/2013
A/Anhui/1/2013
A/Shanghai/1/2013 D Y
A/Hangzhou/1/2013
A/Zhejiang/DTID-ZJU01/2013
A/Hangzhou/2/2013
A/Hangzhou/3/2013
A/Shanghai/3/2013 H
A/Shanghai/4/2013
A/Zhejiang/01/2013
A/Zhejiang/1/2013
A/Zhejiang/2/2013
A/Taiwan/1/2013 N
A/Fujian/1/2013
A/Shanghai/4664T/2013 H
A/Shanghai/Patient3/2013 T M
A/Taiwan/S02076/2013
A/Taiwan/T02081/2013
A/Zhejiang/HZ1/2013
A/Nanjing/1/2013
A/Nanchang/1/2013
A/Huzhou/1/2013
A/Huzhou/10/2013
A/Huzhou/3/2013
A/Huzhou/4/2013
A/Huzhou/5/2013
A/Huzhou/6/2013
A/Wuxi/1/2013
A/Wuxi/2/2013
A/environment/Wuxi/1/2013
A/Jiangsu/1/2013
300 310 320 1 10 20
Consensus LPFQNIDSRAVGKCPRYVKQRSLLLATGMKNVPEIPKGRGLFGAIAGFIENGWEGLIDGW
A/Shanghai/2/2013
A/Anhui/1/2013
A/Shanghai/1/2013
A/Hangzhou/1/2013
A/Zhejiang/DTID-ZJU01/2013
A/Hangzhou/2/2013
A/Hangzhou/3/2013
A/Shanghai/3/2013
A/Shanghai/4/2013
A/Zhejiang/01/2013
A/Zhejiang/1/2013
A/Zhejiang/2/2013
A/Taiwan/1/2013
A/Fujian/1/2013
A/Shanghai/4664T/2013
A/Shanghai/Patient3/2013 G
A/Taiwan/S02076/2013
A/Taiwan/T02081/2013
A/Zhejiang/HZ1/2013
A/Nanjing/1/2013
A/Nanchang/1/2013
A/Huzhou/1/2013
A/Huzhou/10/2013
A/Huzhou/3/2013
A/Huzhou/4/2013
A/Huzhou/5/2013 G
A/Huzhou/6/2013
A/Wuxi/1/2013 N
A/Wuxi/2/2013
A/environment/Wuxi/1/2013
A/Jiangsu/1/2013

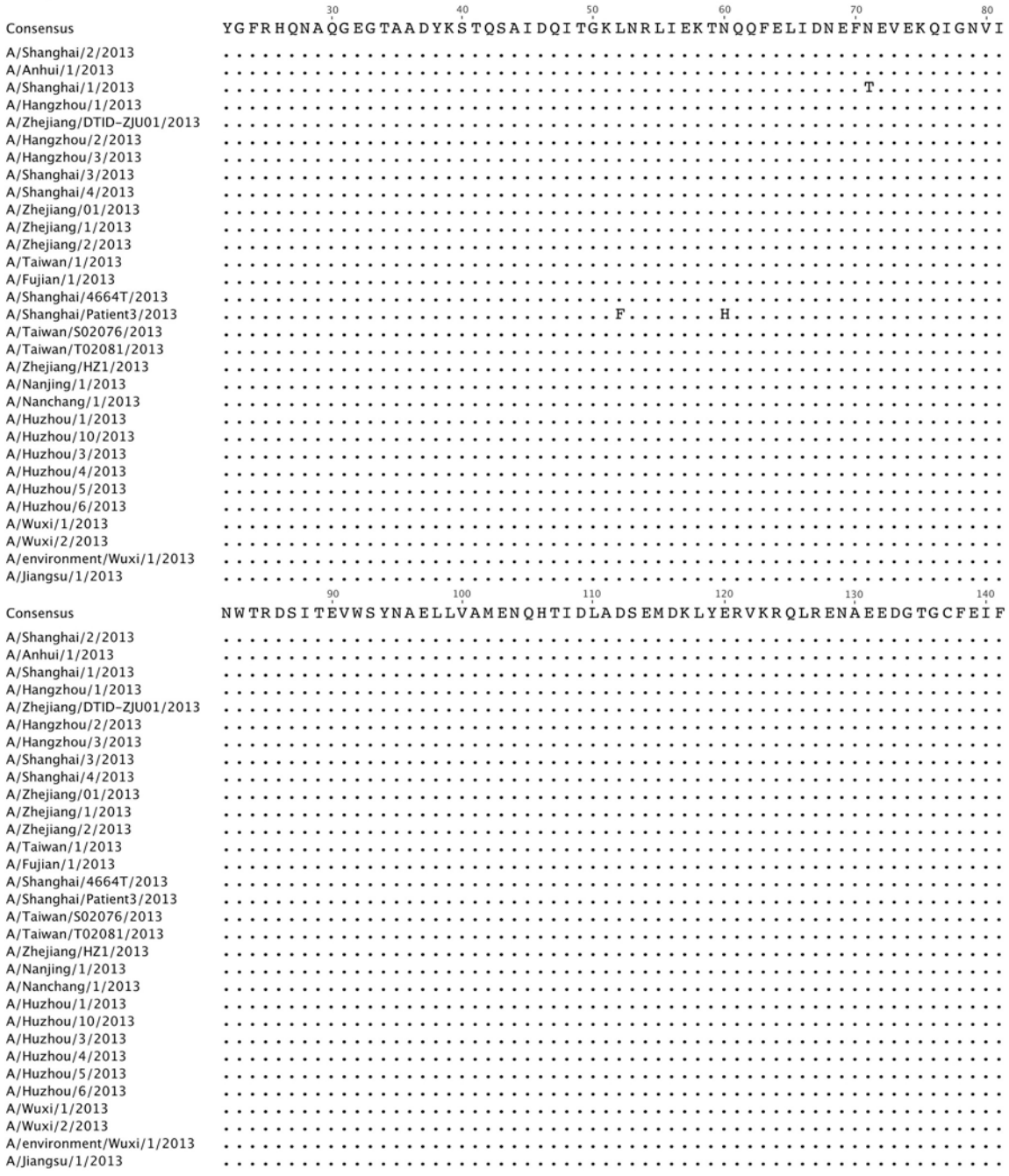
30 40 50 60 70 80
Consensus YGFRHQNAQGEGTAADYKSTQSAIDQITGKLNRLIEKTNQQFELIDNEFNEVEKQIGNVI
A/Shanghai/2/2013
A/Anhui/1/2013
A/Shanghai/1/2013 T
A/Hangzhou/1/2013
A/Zhejiang/DTID-ZJU01/2013
A/Hangzhou/2/2013
A/Hangzhou/3/2013
A/Shanghai/3/2013
A/Shanghai/4/2013
A/Zhejiang/01/2013
A/Zhejiang/1/2013
A/Zhejiang/2/2013
A/Taiwan/1/2013
A/Fujian/1/2013
A/Shanghai/4664T/2013
A/Shanghai/Patient3/2013 F H
A/Taiwan/S02076/2013
A/Taiwan/T02081/2013
A/Zhejiang/HZ1/2013
A/Nanjing/1/2013
A/Nanchang/1/2013
A/Huzhou/1/2013
A/Huzhou/10/2013
A/Huzhou/3/2013
A/Huzhou/4/2013
A/Huzhou/5/2013
A/Huzhou/6/2013
A/Wuxi/1/2013
A/Wuxi/2/2013
A/environment/Wuxi/1/2013
A/Jiangsu/1/2013
90 100 110 120 130 140
Consensus NWTRDSITEVWSYNAELLVAMENQHTIDLADSEMDKLYERVKRQLRENAEEDGTGCFEIF
A/Shanghai/2/2013
A/Anhui/1/2013
A/Shanghai/1/2013
A/Hangzhou/1/2013
A/Zhejiang/DTID-ZJU01/2013
A/Hangzhou/2/2013
A/Hangzhou/3/2013
A/Shanghai/3/2013
A/Shanghai/4/2013
A/Zhejiang/01/2013
A/Zhejiang/1/2013
A/Zhejiang/2/2013
A/Taiwan/1/2013
A/Fujian/1/2013
A/Shanghai/4664T/2013
A/Shanghai/Patient3/2013
A/Taiwan/S02076/2013
A/Taiwan/T02081/2013
A/Zhejiang/HZ1/2013
A/Nanjing/1/2013
A/Nanchang/1/2013
A/Huzhou/1/2013
A/Huzhou/10/2013
A/Huzhou/3/2013
A/Huzhou/4/2013
A/Huzhou/5/2013
A/Huzhou/6/2013
A/Wuxi/1/2013
A/Wuxi/2/2013
A/environment/Wuxi/1/2013
A/Jiangsu/1/2013

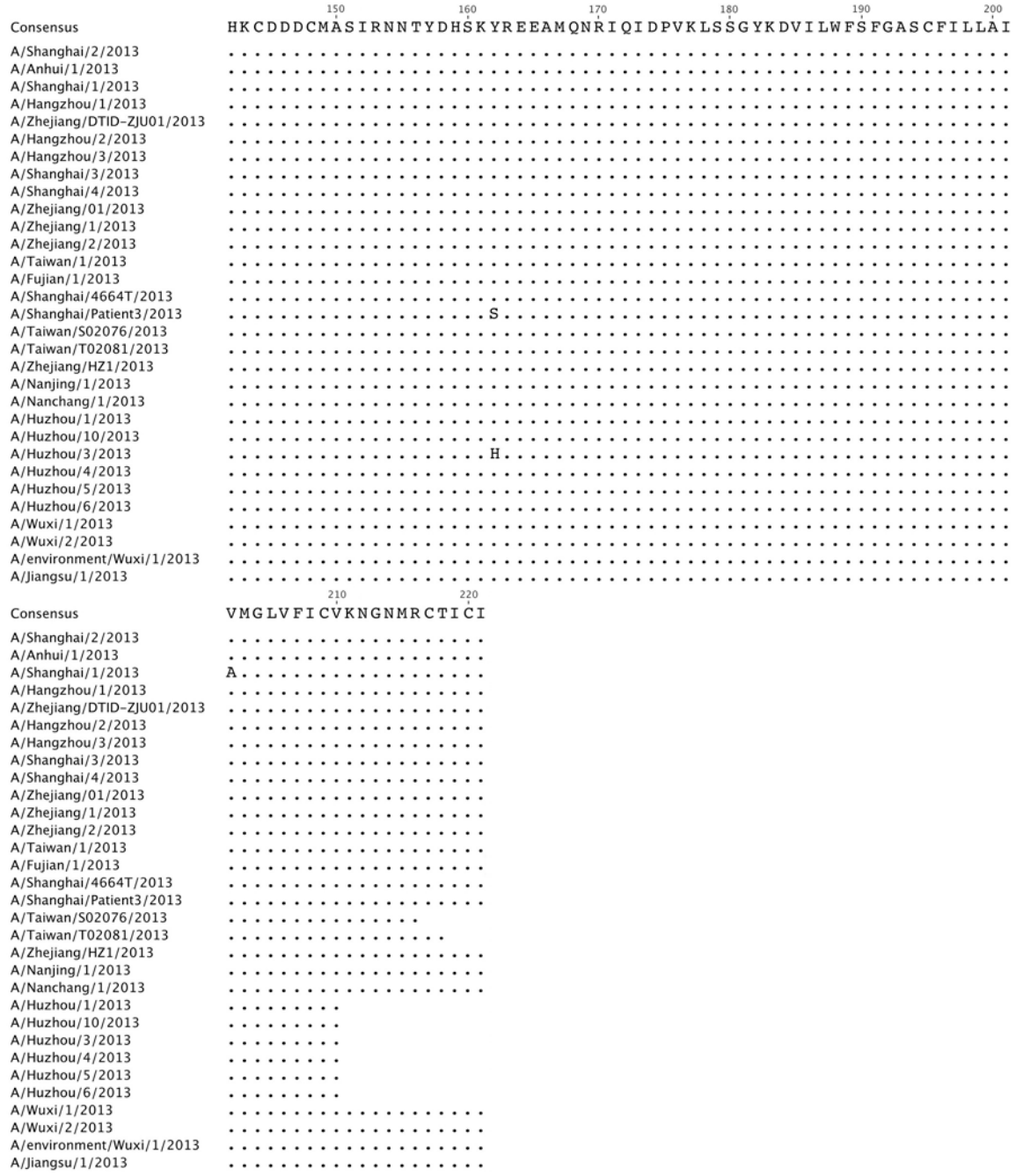

Fig. S5. Sequence alignment of full-length H7N9 HA sequences deposited in Global Initiative on Sharing All Influenza Data (GISAID).

Table S1. Data collection and refinement statistics for Sh2 H7 HA and glycan complexes

	H7 HA	H7 HA	H7 HA	H7 HA
Ligand	*apo*	LSTa	LSTa	LSTc
Soaking condition		10mM, 10min	16mM, 2 hours	10mM, 10min
Data collection				
Beamline	SSRL 12-2	SSRL 12-2	APS 23ID-B	SSRL 12-2
Wavelength (Å)	1.0000	1.0000	1.0331	1.0000
Space group	$P2_13$	$P2_13$	$P2_13$	$P2_13$
Unit cell parameters (Å, °)	a = b = c = 154.5 α = β = γ = 90	a = b = c = 154.7 α = β = γ = 90	a = b = c = 153.9 α = β = γ = 90	a = b = c = 154.8 α = β = γ = 90
Resolution (Å)	50-2.70 (2.80-2.70) [a]	50-2.70 (2.80-2.70)	50-2.60 (2.69-2.60)	50-2.90 (3.00-2.90)
Observations	223,195	187,164	234,550	183,548
Unique reflections	33,899 (3,363)	33,887 (3,362)	37,501 (3,705)	27,559 (2,712)
Completeness (%)	99.8 (100.0)	99.8 (99.9)	99.9 (100.0)	99.9 (100.0)
$\langle I/\sigma_I \rangle$	19.2 (2.6)	19.6 (2.2)	16.9 (2.1)	18.0 (2.8)
R_{sym} (%) [b]	8.9 (75.7)	7.6 (86.3)	9.8 (94.0)	10.6 (93.5)
R_{pim} (%) [c]	3.8 (30.8)	3.4 (38.4)	4.0 (37.1)	4.5 (34.2)
Z_a [d]	2	2	2	2
Refinement				
Resolution (Å)	46.6 -2.70	48.9 -2.70	48.7 -2.60	46.7 -2.90
Reflections (total)	33,870	33,863	37,471	27,534
Reflections (test)	1,718	1,718	1,873	1,385
R_{cryst} (%) [e]	22.9	22.7	21.3	22.6
R_{free} (%) [f]	27.7	26.7	25.9	26.2
Average B-value (Å^2)	100	122	105	119
Protein: protomer 1	59	80	72	73
Protein: protomer 2	141	163	139	166
Wilson B-value (Å^2)	63	68	67	72
Protein atoms	7,600	7,600	7,600	7,600
Carbohydrate atoms	129	132	132	143
Waters	105	35	67	56
RMSD from ideal geometry				
Bond length (Å)	0.002	0.004	0.005	0.003
Bond angles (°)	0.67	0.82	0.93	0.76
Ramachandran statistics (%) [g]				
Favored	94.0	94.0	93.0	93.0
Outliers	1.0	1.3	1.3	1.0
PDB code	4N5J	4N5K	4N61	4N60

Table S2. Data collection and refinement statistics for Sh2 HA glycan complexes

	H7 HA	H7 HA	H7 HA
Ligand	glycan #3	glycan #21	glycan #23
Soaking condition	10mM, 2 hours	10mM, 2 hours	10mM, 2 hours
Data collection			
Beamline	APS 23ID-B	APS 23ID-B	APS 23ID-B
Wavelength (Å)	1.0331	1.0331	1.0331
Space group	$P2_13$	$P2_13$	$P2_13$
Unit cell parameters (Å, °)	a = b = c = 153.8 α = β = γ = 90	a = b = c = 153.6 α = β = γ = 90	a = b = c = 153.9 α = β = γ = 90
Resolution (Å)	50-2.50 (2.59-2.50) [a]	50-2.75 (2.85-2.75)	50-2.70 (2.80-2.70)
Observations	392,387	137,382	209,938
Unique reflections	42,019 (4,158)	31,335 (3,134)	33,536 (3,330)
Completeness (%)	100.0 (100.0)	99.1 (100.0)	100.0 (100.0)
$\langle I/\sigma_I \rangle$	25.1 (3.3)	14.7 (1.9)	16.3 (2.5)
R_{sym} (%) [b]	8.9 (77.2)	9.5 (79.4)	11.2 (77.9)
R_{pim} (%) [c]	2.8 (25.3)	4.8 (36.8)	4.6 (33.9)
Za [d]	2	2	2
Refinement			
Resolution (Å)	48.6 -2.50	42.6 -2.75	48.7 -2.70
Reflections (total)	41,990	31,323	33,505
Reflections (test)	2,121	1,584	1,695
R_{cryst} (%) [e]	23.0	21.6	22.5
R_{free} (%) [f]	26.7	26.5	26.5
Average B-value (Å^2)	101	98	95
Protein: protomer 1	67	68	52.
Protein: protomer 2	133	126	136
Wilson B-value (Å^2)	53	64	54.
Protein atoms	7,600	7,600	7,600
Carbohydrate atoms	181	215	172
Waters	100	79	178
RMSD from ideal geometry			
Bond length (Å)	0.004	0.003	0.003
Bond angles (°)	0.79	0.75	0.79
Ramachandran statistics (%) [g]			
Favored	93.0	93.0	93.0
Outliers	1.3	0.6	1.3
PDB code	4N62	4N63	4N64

[a] Numbers in parentheses refer to the highest resolution shell.

[b] $R_{sym} = \Sigma_{hkl} \Sigma_i | I_{hkl,i} - \langle I_{hkl} \rangle | / \Sigma_{hkl} \Sigma_i I_{hkl,i}$, where $I_{hkl,i}$ is the scaled intensity of the i^{th} measurement of reflection h, k, l, and $\langle I_{hkl} \rangle$ is the average intensity for that reflection.

[c] $R_{pim} = \Sigma_{hkl} (1/(n-1))^{1/2} \Sigma_i | I_{hkl,i} - \langle I_{hkl} \rangle | / \Sigma_{hkl} \Sigma_i I_{hkl,i}$, where n is the redundancy.

[d] Z_a is the number of HA protomers per crystallographic asymmetric unit.

[e] $R_{cryst} = \Sigma_{hkl} | F_o - F_c | / \Sigma_{hkl} | F_o |$ x 100

[f] R_{free} was calculated as for R_{cryst}, but on a test set of 5% of the data excluded from refinement.
[g] Calculated using Molprobity (*47*).

Table S3. Glycans imprinted on the microarray.

Glycan #	Name	Structure
1	Galβ(1-4)-GlcNAcβ-ethyl-NH_2	
2	Galβ(1-4)-GlcNAcβ(1-2)-Manα(1-3)[Galβ(1-4)-GlcNAcβ(1-2)-Manα(1-6)]-Manβ(1-4)-GlcNAcβ(1-4)-GlcNAcβ-Asn-NH_2	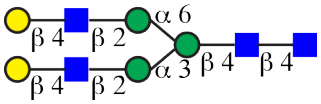
3	NeuAcα(2-3)-Galβ(1-4)-6-O-sulfo-GlcNAcβ-propyl-NH_2	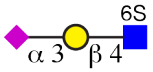
4	NeuAcα(2-3)-Galβ(1-4)-[Fucα(1-3)]-6-O-sulfo-GlcNAcβ-propyl-NH_2	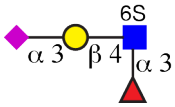
5	NeuAcα(2-3)-6-O-sulfo-Galβ(1-4)-GlcNAcβ-ethyl-NH_2	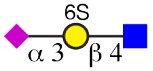
6	NeuAcα(2-3)-6-O-sulfo-Galβ(1-4)-[Fucα(1-3)]-GlcNAcβ-propyl-NH_2	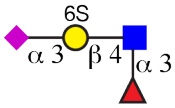
7	NeuAcα(2-3)-Galβ(1-3)-6-O-sulfo-GlcNAcβ-propyl-NH_2	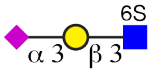
8	NeuAcα(2-3)-Galβ(1-4)-Glcβ-ethyl-NH_2	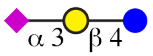
9	NeuAcα(2-3)-Galβ(1-4)-GlcNAcβ-ethyl-NH_2	
10	NeuAcα(2-3)-Galβ(1-4)-GlcNAcβ(1-3)-Galβ(1-4)-GlcNAcβ-ethyl-NH_2	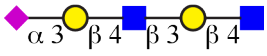
11	NeuAcα(2-3)-Galβ(1-4)-GlcNAcβ(1-3)-Galβ(1-4)-GlcNAcβ(1-3)-Galβ(1-4)-GlcNAcβ-ethyl-NH_2	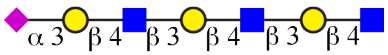
12	NeuAcα(2-3)-GalNAcβ(1-4)-GlcNAcβ-ethyl-NH_2	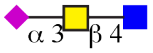
13	NeuAcα(2-3)-Galβ(1-3)-GlcNAcβ-ethyl-NH_2	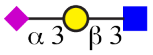
14	NeuAcα(2-3)-Galβ(1-3)-GlcNAcβ(1-3)-Galβ(1-4)-GlcNAcβ-ethyl-NH_2	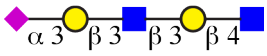
15	NeuAcα(2-3)-Galβ(1-3)-GlcNAcβ(1-3)-Galβ(1-3)-GlcNAcβ-ethyl-NH_2	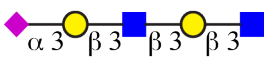
16	NeuAcα(2-3)-Galβ(1-3)-GalNAcβ(1-3)-Galα(1-4)-Galβ(1-4)-Glcβ-ethyl-NH_2	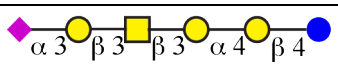
17	NeuAcα(2-3)-Galβ(1-3)-GalNAcα-Thr-NH_2	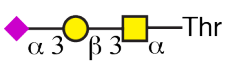
18	NeuAcα(2-3)-Galβ(1-3)-[GlcNAcβ(1-6)]-GalNAcα-Thr-NH_2	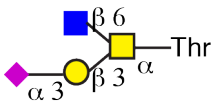

Glycan #	Name	Structure
19	NeuAcα(2-3)-Galβ(1-4)-GlcNAcβ(1-6)-[Galβ(1-3)]-GalNAcα-Thr-NH_2	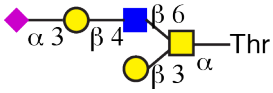
20	NeuAcα(2-3)-Galβ(1-4)-GlcNAcβ(1-3)-Galβ(1-4)-GlcNAcβ(1-6)-[Galβ(1-3)]-GalNAcα-Thr-NH_2	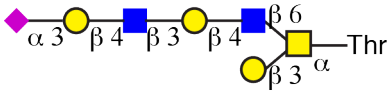
21	NeuAcα(2-3)-Galβ(1-4)-GlcNAcβ(1-3)-GalNAcα-Thr-NH_2	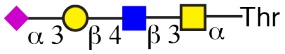
22	NeuAcα(2-3)-Galβ(1-4)-GlcNAcβ(1-3)-Galβ(1-4)-GlcNAcβ(1-3)-GalNAcα-Thr-NH_2	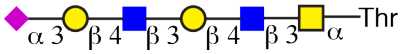
23	NeuAcα(2-3)-Galβ(1-4)-GlcNAcβ(1-3)-[NeuAcα(2-3)-Galβ(1-4)-GlcNAcβ(1-6)]-GalNAcα-Thr-NH_2	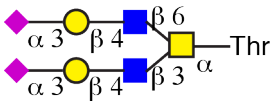
24	NeuAcα(2-3)-Galβ(1-4)-GlcNAcβ(1-3)-Galβ(1-4)-GlcNAcβ(1-3)-[NeuAcα(2-3)-Galβ(1-4)-GlcNAcβ(1-3)-Galβ(1-4)-GlcNAcβ(1-6)]-GalNAcα-Thr-NH_2	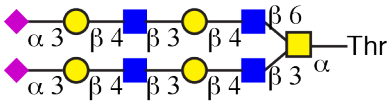
25	NeuAcα(2-3)-Galβ(1-4)-GlcNAcβ(1-2)-Manα(1-3)-[NeuAcα(2-3)-Galβ(1-4)-GlcNAcβ(1-2)-Manα(1-6)]-Manβ(1-4)-GlcNAcβ(1-4)-GlcNAcβ-Asn-NH_2	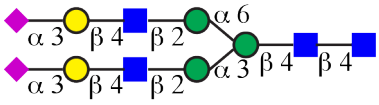
26	NeuAcα(2-3)-Galβ(1-4)-GlcNAcβ(1-3)-Galβ(1-4)-GlcNAcβ(1-2)-Manα(1-3)-[NeuAcα(2-3)-Galβ(1-4)-GlcNAcβ(1-3)-Galβ(1-4)-GlcNAcβ(1-2)-Manα(1-6)]-Manβ(1-4)-GlcNAcβ(1-4)-GlcNAcβ-Asn-NH_2	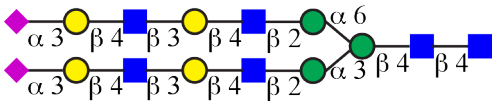
27	NeuAcα(2-3)-Galβ(1-4)-GlcNAcβ(1-3)-Galβ(1-4)-GlcNAcβ(1-3)-Galβ(1-4)-GlcNAcβ(1-2)-Manα(1-3)-[NeuAcα(2-3)-Galβ(1-4)-GlcNAcβ(1-3)-Galβ(1-4)-GlcNAcβ(1-3)-Galβ(1-4)-GlcNAcβ(1-2)-Manα(1-6)]-Manβ(1-4)-GlcNAcβ(1-4)-GlcNAcβ-Asn-NH_2	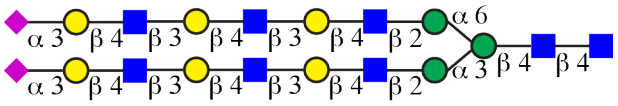
28	NeuAcα(2-3)-[GalNAcβ(1-4)]-Galβ(1-4)-GlcNAcβ-ethyl-NH_2	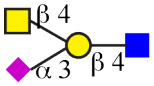
29	NeuAcα(2-3)-[GalNAcβ(1-4)]-Galβ(1-4)-Glcβ-ethyl-NH_2	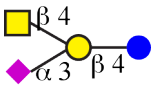
30	Galβ(1-3)-GalNAcβ(1-4)-[NeuAcα(2-3)]-Galβ(1-4)-Glcβ-ethyl-NH_2	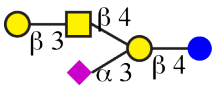
31	NeuAcα(2-3)-Galβ(1-4)-[Fucα(1-3)]-GlcNAcβ-propyl-NH_2	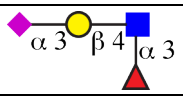

Glycan #	Name	Structure
32	NeuAcα(2-3)-Galβ(1-3)-[Fucα(1-4)]-GlcNAcβ(1-3)-Galβ(1-4)-[Fucα(1-3)]-GlcNAcβ-ethyl-NH_2	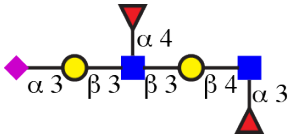
33	NeuAcα(2-3)-Galβ(1-4)-[Fucα(1-3)]-GlcNAcβ(1-3)-Galβ(1-4)-[Fucα(1-3)]-GlcNAcβ-ethyl-NH_2	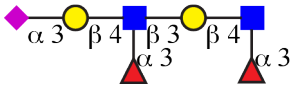
34	NeuAcα(2-3)-Galβ(1-4)-[Fucα(1-3)]-GlcNAcβ(1-3)-Galβ(1-4)-[Fucα(1-3)]-GlcNAcβ(1-3)-Galβ(1-4)-[Fucα(1-3)]-GlcNAcβ-ethyl-NH_2	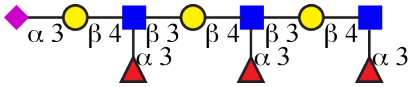
35	NeuGcα(2-3)-Galβ(1-4)-GlcNAcβ-ethyl-NH_2	
36	NeuAcα(2-6)-Galβ(1-4)-6-O-sulfo-GlcNAcβ-propyl-NH_2	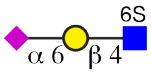
37	NeuAcα(2-6)-Galβ(1-4)-Glcβ-ethyl-NH_2	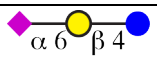
38	NeuAcα(2-6)-Galβ(1-4)-GlcNAcβ-ethyl-NH_2	
39	NeuAcα(2-6)-Galβ(1-4)-GlcNAcβ(1-3)-Galβ(1-4)-GlcNAcβ-ethyl-NH_2	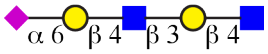
40	NeuAcα(2-6)-Galβ(1-4)-GlcNAcβ(1-3)-Galβ(1-4)-GlcNAcβ(1-3)-Galβ(1-4)-GlcNAcβ-ethyl-NH_2	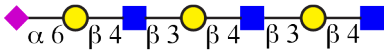
41	NeuAcα(2-6)-Galβ(1-4)-GlcNAcβ(1-3)-[NeuAcα(2-6)]-Galβ(1-4)-GlcNAcβ-ethyl-NH_2	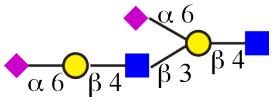
42	NeuAcα(2-6)-GalNAcβ(1-4)-GlcNAcβ-ethyl-NH_2	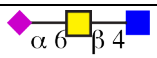
43	NeuAcα(2-6)-[Galβ(1-3)]-GalNAcα-Thr-NH_2	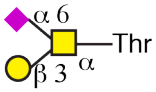
44	NeuAcα(2-6)-Galβ(1-4)-GlcNAcβ(1-6)-[Galβ(1-3)]-GalNAcα-Thr-NH_2	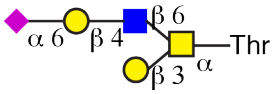
45	NeuAcα(2-6)-Galβ(1-4)-GlcNAcβ(1-3)-Galβ(1-4)-GlcNAcβ(1-6)-[Galβ(1-3)]-GalNAcα-Thr-NH_2	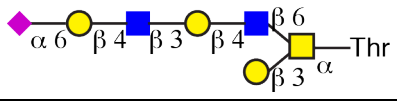
46	NeuAcα(2-6)-Galβ(1-4)-GlcNAcβ(1-3)-GalNAcα-Thr-NH_2	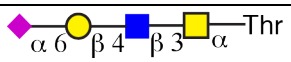
47	NeuAcα(2-6)-Galβ(1-4)-GlcNAcβ(1-3)-Galβ(1-4)-GlcNAcβ(1-3)-GalNAcα-Thr-NH_2	
48	NeuAcα(2-6)-Galβ(1-4)-GlcNAcβ(1-3)-[NeuAcα(2-6)-Galβ(1-4)-GlcNAcβ(1-6)]-GalNAcα-Thr-NH_2	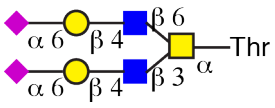

Glycan #	Name	Structure
49	NeuAcα(2-6)-Galβ(1-4)-GlcNAcβ(1-3)-Galβ(1-4)-GlcNAcβ(1-3)-[NeuAcα(2-6)-Galβ(1-4)-GlcNAcβ(1-3)-Galβ(1-4)-GlcNAcβ(1-6)]-GalNAcα-Thr-NH_2	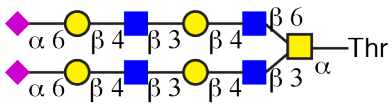
50	Galβ(1-4)-GlcNAcβ(1-2)-Manα(1-3)-[NeuAcα(2-6)-Galβ(1-4)-GlcNAcβ(1-2)-Manα(1-6)]-Manβ(1-4)-GlcNAcβ(1-4)-GlcNAcβ-Asn-NH_2	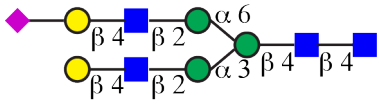
51	NeuAcα(2-6)-Galβ(1-4)-GlcNAcβ(1-2)-Manα(1-3)-[Galβ(1-4)-GlcNAcβ(1-2)-Manα(1-6)]-Manβ(1-4)-GlcNAcβ(1-4)-GlcNAcβ-Asn-NH_2	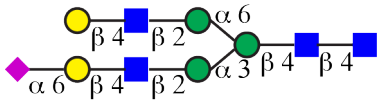
52	GlcNAcβ(1-2)-Manα(1-3)-[NeuAcα(2-6)-Galβ(1-4)-GlcNAcβ(1-2)-Manα(1-6)]-Manβ(1-4)-GlcNAcβ(1-4)-GlcNAcβ-Asn-NH_2	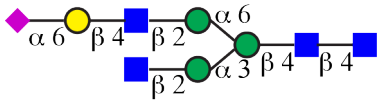
53	NeuAcα(2-6)-Galβ(1-4)-GlcNAcβ(1-2)-Manα(1-3)-[NeuAcα(2-6)-Galβ(1-4)-GlcNAcβ(1-2)-Manα(1-6)]-Manβ(1-4)-GlcNAcβ(1-4)-GlcNAcβ-Asn-NH_2	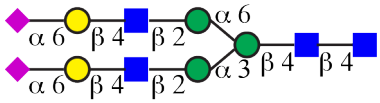
54	NeuAcα(2-6)-Galβ(1-4)-GlcNAcβ(1-3)-Galβ(1-4)-GlcNAcβ(1-2)-Manα(1-3)-[NeuAcα(2-6)-Galβ(1-4)-GlcNAcβ(1-3)-Galβ(1-4)-GlcNAcβ(1-2)-Manα(1-6)]-Manβ(1-4)-GlcNAcβ(1-4)-GlcNAcβ-Asn-NH_2	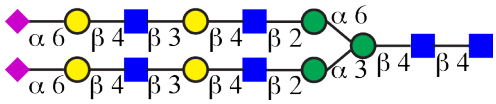
55	NeuAcα(2-6)-Galβ(1-4)-GlcNAcβ(1-3)-Galβ(1-4)-GlcNAcβ(1-3)-Galβ(1-4)-GlcNAcβ(1-2)-Manα(1-3)-[NeuAcα(2-6)-Galβ(1-4)-GlcNAcβ(1-3)-Galβ(1-4)-GlcNAcβ(1-3)-Galβ(1-4)-GlcNAcβ(1-2)-Manα(1-6)]-Manβ(1-4)-GlcNAcβ(1-4)-GlcNAcβ-Asn-NH_2	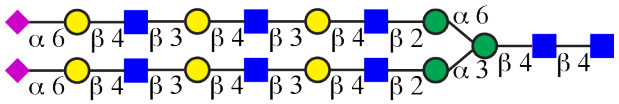
56	NeuGcα(2-6)-Galβ(1-4)-GlcNAcβ-ethyl-NH_2	
57	NeuAcα(2-3)-Galβ(1-4)-GlcNAcβ(1-2)-Manα(1-3)-[NeuAcα(2-6)-Galβ(1-4)-GlcNAcβ(1-2)-Manα(1-6)]-Manβ(1-4)-GlcNAcβ(1-4)-GlcNAcβ-Asn-NH_2	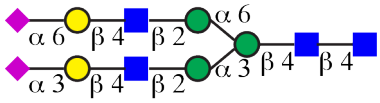
58	NeuAcα(2-6)-Galβ(1-4)-GlcNAcβ(1-2)-Manα(1-3)-[NeuAcα(2-3)-Galβ(1-4)-GlcNAcβ(1-2)-Manα(1-6)]-Manβ(1-4)-GlcNAcβ(1-4)-GlcNAcβ-Asn-NH_2	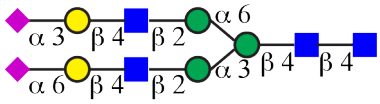

Supporting references

40. Z. Otwinowski, W. Minor, Processing of X-ray diffraction data collected in oscillation mode. *Meth. Enzymol.* **276**, 307 (1997).
41. A. J. McCoy, R. W. Grosse-Kunstleve, L. C. Storoni, R. J. Read, Likelihood-enhanced fast translation functions. *Acta Cryst.* **D61**, 458 (2005).
42. P. D. Adams *et al.*, PHENIX: building new software for automated crystallographic structure determination. *Acta Cryst.* **D58**, 1948 (2002).
43. P. Emsley, K. Cowtan, Coot: model-building tools for molecular graphics. *Acta Cryst.* **D60**, 2126 (2004).
44. R. P. de Vries *et al.*, Only two residues are responsible for the dramatic difference in receptor binding between swine and new pandemic H1 hemagglutinin. *J. Biol. Chem.* **286**, 5868 (2011).
45. P. B. Harbury, T. Zhang, P. S. Kim, T. Alber, A switch between two-, three-, and four-stranded coiled coils in GCN4 leucine zipper mutants. *Science* **262**, 1401 (1993).
46. R. P. de Vries *et al.*, The influenza A virus hemagglutinin glycosylation state affects receptor-binding specificity. *Virology* **403**, 17 (2010).
47. I. W. Davis *et al.*, MolProbity: all-atom contacts and structure validation for proteins and nucleic acids. *Nucleic Acids Res.* **35**, W375 (2007).